REGULAR ARTICLE

blood advances

Type 2M/2A von Willebrand disease: a shared phenotype between type 2M and 2A

Omid Seidizadeh,[1] Luca Mollica,[2] Serena Zambarbieri,[2] Luciano Baronciani,[3] Andrea Cairo,[3] Paola Colpani,[3] Giovanna Cozzi,[3] Maria Teresa Pagliari,[3] Alessandro Ciavarella,[3] Simona M. Siboni,[3] and Flora Peyvandi[1,3]

[1]Department of Pathophysiology and Transplantation and [2]Department of Medical Biotechnologies and Translational Medicine, Università degli Studi di Milano, Milan, Italy; and [3]Fondazione IRCCS Ca'Granda Ospedale Maggiore Policlinico, Angelo Bianchi Bonomi Hemophilia and Thrombosis Center, Milan, Italy

Key Points

- Four *VWF* variants have been subjected to debate and received different VWD classifications: p.R1315L, p.R1315C, p.R1374H, and p.R1374C.
- We propose a new classification of VWD type 2M/2A for p.R1315L, p.R1374H, and p.R1374C because they share a common phenotype with 2M and 2A.

Four variants have been continuously subjected to debate and received different von Willebrand disease (VWD) classifications: p.R1315L, p.R1315C, p.R1374H, and p.R1374C. We chose to comprehensively investigate these variants with full set of VWD tests, protein-modeling predictions and applying structural biology. Patients with p.R1315L, p.R1315C, p.R1374H, and p.R1374C were included. A group with type 2A and 2M was included to better understand similarities and differences. Patients were investigated for phenotypic assays and underlying disease mechanisms. We applied deep protein modeling predictions and structural biology to elucidate the causative effects of variants. Forty-three patients with these variants and 70 with 2A (n = 35) or 2M (n = 35) were studied. Patients with p.R1315L, p.R1374H, or p.R1374C showed a common phenotype between 2M and 2A using von Willebrand factor (VWF):GPIbR/VWF:Ag and VWF:CB/VWF:Ag ratios and VWF multimeric profile, whereas p.R1315C represented a type 2M phenotype. There was an overall reduced VWF synthesis or secretion in 2M and cases with p.R1315L, p.R1374H, and p.R1374C, but not in 2A. Reduced VWF survival was observed in most 2A (77%), 2M (80%), and all 40 cases with p.R1315L, p.R1374H, and p.R1374C. These were the only variants that fall at the interface between the A1-A2 domains. p.R1315L/C mutants induce more compactness and internal mobility, whereas p.R1374H/C display a more extended overall geometry. We propose a new classification of type 2M/2A for p.R1315L, p.R1374H, and p.R1374C because they share a common phenotype with 2M and 2A. Our structural analysis shows the unique location of these variants on the A1-A2 domains and their distinctive effect on VWF.

Introduction

von Willebrand disease (VWD), with an estimated prevalence of ~1% in the general population, is believed to be the most common congenital bleeding disorder.[1-4] Using population-based genetic study, a higher possible prevalence has even been established.[5] VWD results from a variety of quantitative or qualitative defects in the von Willebrand factor (VWF) glycoprotein. Quantitative deficiencies are responsible for type 1 with a partial decrease and type 3 with the complete absence of VWF. VWF qualitative abnormalities cause type 2 VWD and are further divided into type 2A, 2B, 2M, and 2N.[6,7]

Submitted 10 January 2024; accepted 26 January 2024; prepublished online on *Blood Advances* First Edition 5 February 2024; final version published online 29 March 2024. https://doi.org/10.1182/bloodadvances.2024012626.

Data are available on request from the corresponding author, Flora Peyvandi (flora.peyvandi@unimi.it).

The full-text version of this article contains a data supplement.

Type 2A VWD is characterized by reduced platelet adhesion owing to the lack or reduction of high-molecular weight multimers (HMWM).[7] These patients typically have remarkably low ratios of platelet-dependent VWF activity (VWF activity)/VWF antigen (VWF:Ag) and VWF collagen binding (VWF:CB)/VWF:Ag.[8] Type 2B is characterized by an elevated binding affinity of the A1 domain for the platelet glycoprotein Ib (GPIb), usually leading to a loss of the HMWM and occasionally reduced platelet counts.[7] Patients with this type usually have reduced VWF activity/VWF:Ag and VWF:CB/VWF:Ag ratios, but differently from type 2A, have an increased ristocetin-induced platelet agglutination.[8] 2M is characterized by the reduced affinity of the A1 domain for GPIb or for collagen in the A1 or A3 domain, without a selective deficiency of HMWM.[7] Owing to the defective binding to GPIb, patients with type 2M have a reduced VWF activity/VWF:Ag ratio with a normal VWF:CB/VWF:Ag ratio. However, patients with a defective collagen binding show the opposite pattern.[8] Type 2N is the result of genetic variants located in the D′–D3 domains leading to a defective binding to factor VIII (FVIII) and thus reduced FVIII plasma levels.[7,9]

VWD presents heterogeneous clinical and laboratory manifestations. Patients with the same *VWF* genetic variant may show different bleeding symptoms or even laboratory results.[10,11] Indeed, in our previous investigation of type 2 VWD on 321 patients with a confirmed genetic diagnosis, several patients (excluding type 2N and 2M with collagen-binding defects) had a VWF activity/VWF:Ag ratio of $\geq$0.6 (n = 54) or $\geq$0.7 (n = 34), despite having type 2A, 2B, or 2M.[8] This reflects the heterogeneity of VWD laboratory phenotype. Genetic variants of type 2 are usually penetrant and of straightforward classification. However, their classification sometimes might be challenging and controversial. Among these, 3 *VWF* variants have been continuously subjected to debate and received different VWD classifications: p.R1315L, p.R1315C, p.R1374H, and p.R1374C.

In this study, we took advantage of our large cohort of patients carrying these variants to comprehensively investigate them and also to explore the similarities and differences with archetypal 2M and 2A genetic variants. We further applied deep protein modeling predictions and structural biology to elucidate the underlying causative effects of these variants.

Materials and methods

Patients

All patients who were genetically confirmed to carry p.R1315L, p.R1315C, p.R1374H, and p.R1374C and were referred to the A.B.B Hemophilia and Thrombosis Center were included. To understand the similarities and differences among patients with these variants in comparison with other type 2 VWD, we also included a fully characterized group of patients with type 2A and 2M VWD. Informed consent was obtained from all patients according to the Declaration of Helsinki.

Laboratory measurements

VWF:Ag levels were measured using immunoturbidometric assay (HemosIL von Willebrand Factor Antigen, Instrumentation Laboratory, Bedford, MA). Platelet-dependent VWF activity was measured using VWF:GPIbR (HemosIL von Willebrand Factor Ristocetin Cofactor Activity, Instrumentation Laboratory, Bedford, MA). FVIII clotting activity (FVIII:C) was assessed using a 1-stage assay and VWF collagen binding (VWF:CB) with collagen type I, III, or a combination of thereof using an enzyme-linked immunosorbent assay method.[12] VWF multimer analysis was performed using a semiautomatic Hydrasys 2 scan (Sebia, Lisses, France), and we used the HYDRAGEL 5 von WILLEBRAND MULTIMERS kit.[13] A commercially available enzyme-linked immunosorbent assay kit (Sanquin, Amsterdam, The Netherlands) was used to measure the VWF propeptide (VWFpp) antigen.[14] To evaluate the synthesis and secretion of VWF we used the FVIII:C/VWF:Ag ratio and VWFpp.[14] VWF clearance was assessed using the VWFpp/VWF:Ag ratio with a ratio exceeding 1.6 considered an indicator of accelerated clearance.[15]

Genetic testing

Genomic DNA was extracted using standard methods.[16] The polymerase chain reaction and Sanger sequencing or next-generation sequencing were performed for patients as previously described.[16-18] For all patients diagnosed before 2018, the target sequencing approach was applied to amplify the exon encoding the specific VWF domains, including intron-exon boundaries.[8,15] The sequencing of target exon(s) was based on the biochemical results used to identify the defective VWF domains. For those who were diagnosed after 2018, next-generation sequencing was performed.

Protein modeling and VWF structural analysis

Starting structure model. The starting structure of the A1 (residues 1263-1464) and A2 (residues 1495-1671) domains, connected by an unstructured linker, was reconstructed (A1-A2) on the basis of the existing experimental structures of single domains (A1: PDB ID 7eow[19] A2: PDB ID 7gbx[20]) by means of AlphaFold2 web server[21] (supplemental Figure 1).

Langevin dynamics. The starting structure of A1-A2 (obtained as above) was modeled under the action of internal plus frictional forces in the framework of the Langevin dynamics. For this, we used the generalized Born implicit solvent model[22] as implemented in the Nanoscale Molecular Dynamics code.[23] The system was parametrized using the CHARM22 force field.[24] After a first local geometry optimization, conjugate gradient energy minimization,[24] a 200 ns simulation was performed in the canonical (NVT) ensemble at 300 K with an integration step of 2 fs and a damping coefficient equal to 1 ps^{-1}. The electrostatics were treated with the cutoff scheme (14 Å).

Molecular dynamics. A representative frame corresponding to an average final configuration of the A1-A2 system was extracted from the Langevin dynamics time window that displayed structural convergence, that is, when the overall root mean square deviation (RMSD) of the backbone reaches a plateau (supplemental Figure 1). This structure was considered as the reference wild-type A1-A2 system (wt A1-A2) and was used for performing molecular dynamics (MD) simulations of the wt and of the mutated proteins (p.R1315C, p.R1315L, p.R1374C, and p.R1374H) generated via manual editing of wt A1-A2 in Pymol (https://pymol.org/2/#download). All the systems were parametrized in GROMACS 2020.1[25] using the AMBER99-SB ILDN force field.[26]

A parallelepipedal solvent box was created around the protein, solvated with TIP3P[27] water molecules. The net charge was neutralized, and the electrostatics were treated with the Particle-Mesh-Ewald scheme. After minimization with the steepest descent method[28] (convergence, 100 kJ mol^{-1} nm^{-1}), the system was equilibrated (with isotropic positional restraints on protein heavy atoms, k = 1000 kJ mol^{-1} nm^{-2}) for 2 ns in the NPT ensemble with a pressure of 1 atm and temperature (T) = 300 K, then for 2 ns in the NVT ensemble at T = 300 K. Eventually, we performed 200 ns of simulation for each system in the NVT ensemble using a time-step of 2 fs and constraining all covalent bond lengths with the LINCS algorithm.[29] These analyses were performed using the GROMACS internal programs and routines with the support of an in-house code, and the molecular graphics were visualized using Visual Molecular Dynamics.[30]

Statistical analysis

Continuous variables were described as medians (ranges) and categorical variables as counts (percentages). The Kruskal-Wallis test was applied to assess differences in the VWF values between different VWD types. The Mann-Whitney *U* test was used to compare medians between 2 independent groups and a *P* value < .05 was considered statistically significant. All statistical analyses were performed using SPSS for Windows, version 21.0 (SPSS, Chicago, IL) and R statistical software environment (The R Foundation, Vienna, Austria).

Results

Patients

A total of 43 patients were referred to our center so far with p.R1315C (n = 3), p.R1315L (n = 7, in cis with p.R924Q), p.R1374C (n = 7), and p.R1374H (n = 26) *VWF* variants. We previously confirmed a type 2M diagnosis for p.R1315C [8] with reduced VWF:GPIbR/VWF:Ag, normal VWF:CB/VWF:Ag, and normal multimer profile. Therefore, this variant was classified among the type 2M group of this study, and all phenotypic results reported from now on are on the remaining 40 cases. Of note, we performed the protein modeling predictions for p.R1315C along with the other 3 variants. The current median (range) age of the cohort with p.R1315L, p.R1374H, and p.R1374C was 54 years (12-83), and 65% were males (Table 1). We also included classical type 2A (n = 35) with increased cleavage of VWF A2 domain by ADAMTS13, and classical type 2M (n = 35) with defective GPIb binding of VWF A1 domain. Patients with type 2A and 2M VWD had 13 and 14 different *VWF* genetic variants, accordingly (Table 2).

Laboratory results

The median FVIII:C level in the cohort was similar to that of type 2M (*P* = .61) and 2A (*P* = .62, Table 1). Patients with p.R1315L, p.R1374H, and p.R1374C had lower VWF:Ag compared with type 2A (28 IU/dL vs 45 IU/dL; *P* = .0026) however, with no difference to type 2M (28 IU/dL vs 26 IU/dL; *P* = .24). No differences were found for VWF:GPIbR between the 3 groups with a median of 9 IU/dL, 11 IU/dL, and 10 IU/dL in type 2A, 2M, and the cohort, respectively.

The VWF:GPIbR/VWF:Ag ratio, used to assess the binding activity of VWF to GPIb, was severely reduced in type 2A (median of 0.24) and also in patients with p.R1315L, p.R1374H, and p.R1374C (median, 0.29), with a significant difference between the 2 groups (*P* = .01, Figure 1). In type 2M, the median ratio was significantly higher than that of type 2A (0.45 vs 0.24; *P* < .0001.) and of the cohort (*P* = .006; Figure 1). The VWF:CB/VWF:Ag ratio, an indication of loss of HMWM, was severely reduced in type 2A (median, 0.15), moderately reduced in the cohort (median, 0.52), but was normal in type 2M (median, 0.7). Altogether, these results showed that patients with p.R1315L, p.R1374H, and p.R1374C have a markedly decreased VWF:GPIbR/VWF:Ag ratio but only a mildly decreased VWF:CB/VWF:Ag ratio, suggesting a shared phenotype between type 2M and 2A (Figure 1). Therefore, we further investigated them with multimer analysis to better understand the concentration and distribution of VWF multimers.

VWF multimer analysis

Patients with classical type 2A showed a very low proportion of HMWM, whereas low MWM were largely represented as a consequence of increased VWF cleavage. Figure 2A shows densitometry for patients with type 2A VWD carrying variants p.I1628T, p.S1506L, and p.G1629R. Patients with classical 2M with a defective GPIba binding of A1 domain, primarily displayed a "flat" pattern, in which the HMWM, although quantitatively diminished, still are the predominant forms of VWF multimers. Figure 2B shows densitometry for patients with 2M VWD with variants

Table 1. Demographic data and laboratory results of patients

VWD type	Type 2A (n = 35)	Type 2M (n = 35)	Type 2M/2A* (n = 40)
Age (y)	41 (11-80)	45 (5-76)	54 (12-83)
Sex (male/female)	14/21	14/21	26/14
FVIII:C, IU/dL	49 (21-91)	45 (23-124)	46 (24-133)
VWF:Ag, IU/dL	45 (13-130)	26 (12-130)	28 (12-90)
VWF:GPIbR, IU/dL	9 (3-24)	11 (4-44)	10 (3-23)
VWF:GPIbR/VWF:Ag ratio	0.24 (0.05-0.57)	0.45 (0.14-1.2)	0.29 (0.14-0.68)
VWF:CB, IU/dL	7 (1-26)	17 (8-80)	14 (3-52)
VWF:CB/VWF:Ag ratio	0.15 (0.03-0.44)	0.7 (0.3-1.18)	0.52 (0.1-0.95)

Data are presented as median (range).
*Three patients with variant p.R1315C are classified among type 2M.

Table 2. VWF genetic variants

Type 2A variants (n = 13)	Type 2M variants (n = 14)	Type 2M/2A (n = 3)
p.C1272R (n = 1)*	p.D1277_L1278delinsE (n = 3)	p.R1315L (n = 7)
p.S1506L (n = 3)	p.D1283H (n = 2)	p.R1374H (n = 26)
p.S1517R (n = 2)	p.R1315C (n = 3)	p.R1374C (n = 7)
p.H1536_V1537del (n = 1)	p.Y1321C (n = 2)	
p.T1578N (n = 1)	†p.I1343V-V1360A-F1369I-S1378F-R1379C (n = 2)	
p.I1628N (n = 1)	†p.V1360A-F1369I-S1378F-R1379C (n = 3)	
p.I1628T (n = 4)	†p.F1369I-S1378F-R1379C (n = 3)	
p.G1629R (n = 8)	p.A1377V-R1379C (n = 8)	
p.G1631D (n = 4)	p.R1399C (n = 3)	
p.L1657P (n = 2)	p.K1408del (n = 1)	
p.V1665E (n = 1)	p.G1415D (n = 1)	
p.R1597Q (n = 5)	p.I1416N (n = 2)	
p.R1597W (n = 2)	p.R1426P (n = 1)	
	p.A1437T (n = 1)	

*n indicates number of patients with a given genetic variant.
†Gene conversion.

p.G1415D, p.A1377V-R1379C, and p.V1360A-F1369I-S1378F-R1379C. The multimeric pattern of p.R1315C variant was also similar to that of patients with type 2M (supplemental Figure 2). In patients with p.R1315L, p.R1374H, and p.R1374C variants, we found a distinct multimeric profile with some mixed features with type 2A and 2M. Figure 2C shows densitometry for patients with variants p.R1374C, p.R1374H, and p.R1315L (in cis with p.R924Q). These 3 variants are clearly associated with a slightly quantitative reduction of HMWM and faintly increased low and intermediate VWF multimers, a distinct profile from both type 2A and 2M (supplemental Figure 3).

Underlying mechanisms of type 2A, 2M and p.R1315L, p.R1374H/C variants

VWF synthesis/secretion. FVIII:C/VWF:Ag ratio and VWFpp were used as criteria to assess the synthesis or secretion of VWF.[14] Patients with type 2A had a VWFpp values comparable to

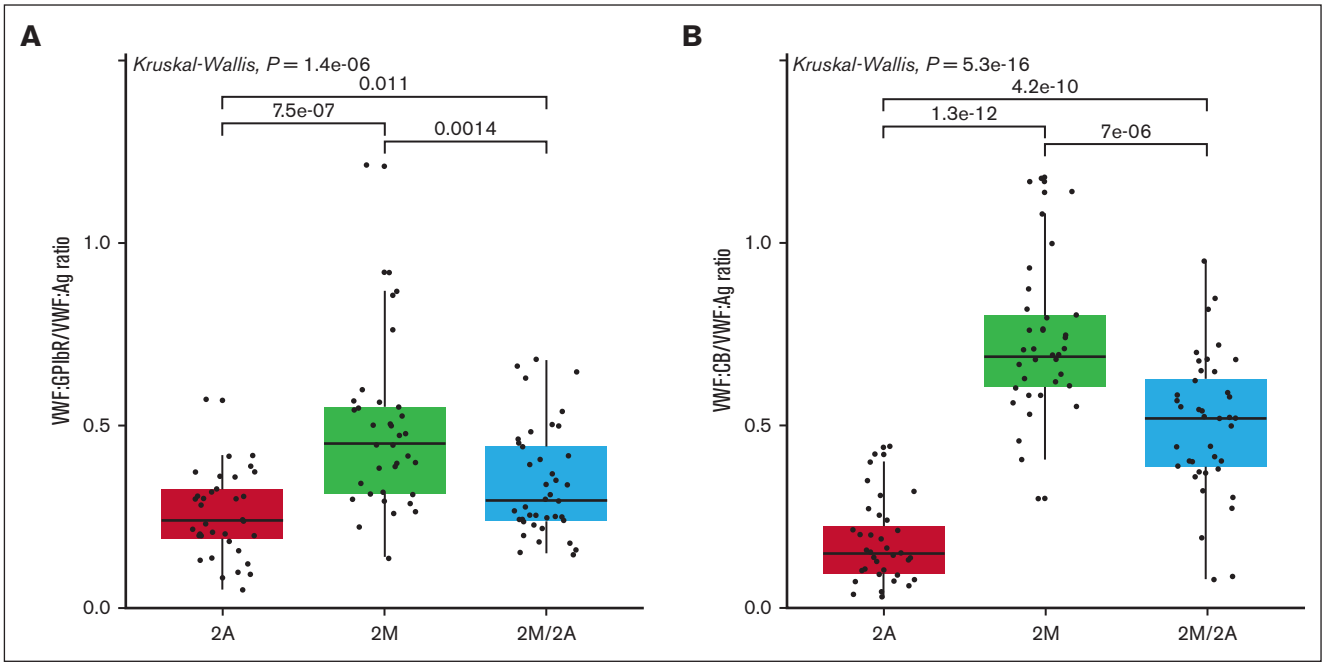

Figure 1. Comparison of von Willebrand factor (VWF) activities to VWF antigen (Ag) ratio in the study population. (A) VWF:GPIbR/VWF:Ag and (B) VWF:CB/VWF:Ag ratios.

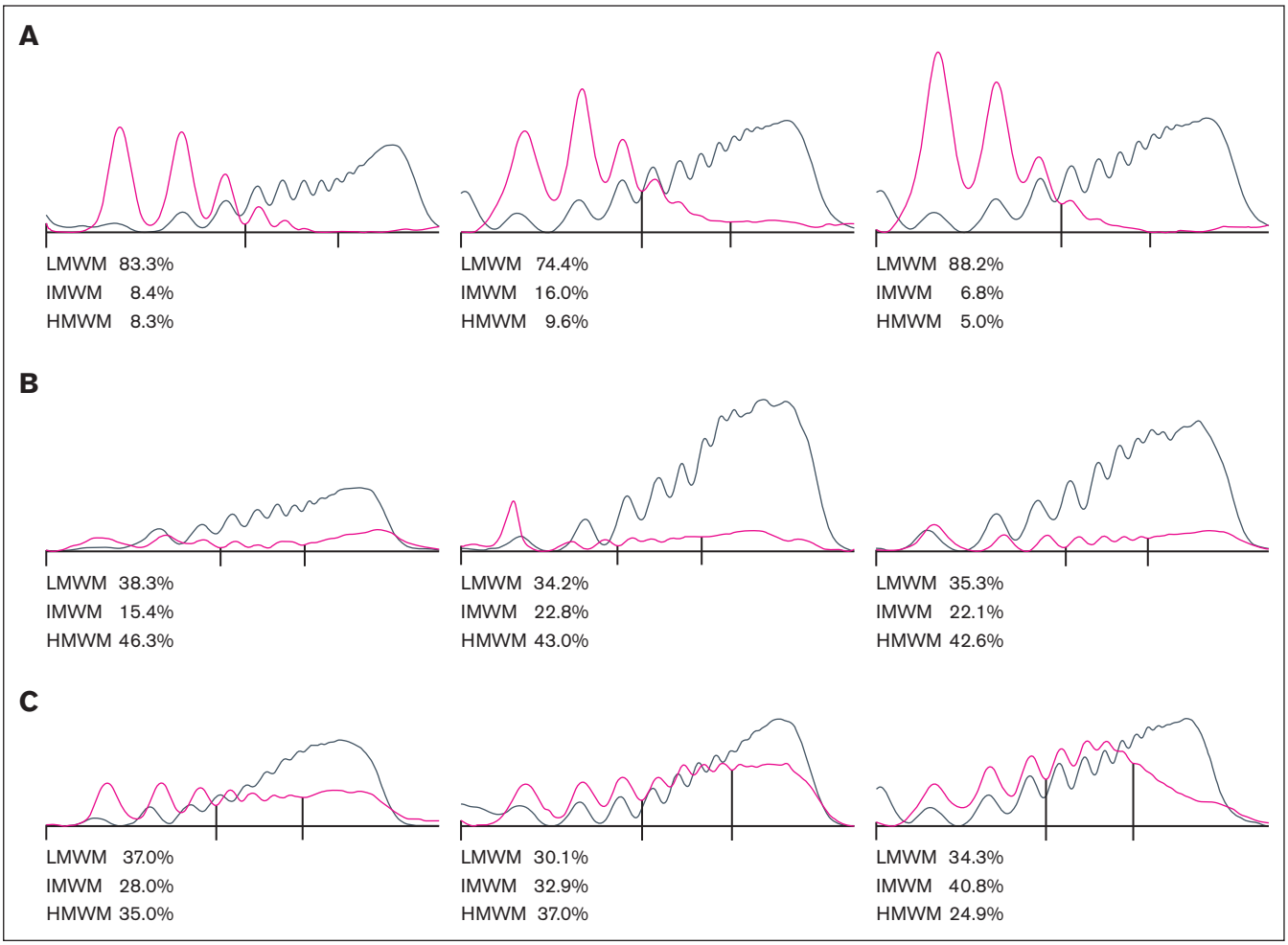

Figure 2. The multimer pattern (densitometric analysis) for patients with type 2 VWD. (A) Densitometry analysis for type 2A patients with variants p.I1628T, p.S1506L, and p.G1629R. Patients with type 2A VWD have a very low level of large VWF multimers, whereas low molecular weight VWF multimers are largely represented. (B) Densitometry analysis for patients with type 2M with variants p.G1415D, p.A1377V-R1379C, and p.V1360A-F1369I-S1378Phe-R1379C. Patients with classical 2M mostly display a "flat" pattern, in which large VWF multimers, although diminished, still are the predominant form. (C) Densitometry analysis for patients with VWD type 2M/2A with variant p.R1374C, p.R1374H, and p.R1315L-R924Q. Type 2M/2A is associated with a slight quantitative reduction of large VWF multimers and increased low and intermediated multimers, distinct from both type 2M and 2A. Densitometric representation of peaks from left to right, with peaks 1 to 3 being low molecular weight, peaks 4 to 7 being intermediate molecular weight, and all other peaks representing high molecular weight multimers. Gray, a pool of normal samples; pink, sample test.

those of healthy controls (80 vs 93 IU/dL; $P = .149$). Similarly, the FVIII:C/VWF:Ag ratio of type 2A was not different from healthy controls (median, 1.16 vs 1.01; $P = .21$). In patients with type 2M, we found a significantly lower VWFpp (64 vs 93 IU/dL; $P < .0001$) and also a higher FVIII:C/VWF:Ag ratio (1.68 vs 1.01; $P < .0001$) compared with healthy controls. Cases with p.R1315L, p.R1374H, and p.R1374C variants, similar to type 2M, showed an overall decreased synthesis of VWF with a median VWFpp value of 74 vs 93 IU/dL of healthy controls ($P < .0001$) and FVIII:C/VWF:Ag ratio of 1.56 vs 1.01 of healthy controls ($P < .0001$). Cumulatively, these results suggest a reduced VWF synthesis or secretion in both type 2M and cases with p.R1315L, p.R1374H, and p.R1374C variants, with no apparent synthesis or secretion defect for type 2A (Figure 3).

VWF clearance. A ratio of >1.6 for VWFpp/VWF:Ag ratio was considered as enhanced VWF clearance.[15] Reduced VWF survival was observed in 77% of patients with type 2A and 80% of those with type 2M. All 40 cases with p.R1315L, p.R1374H, and p.R1374C variants had enhanced VWF clearance with an overall median of 2.5 (range, 1.7-3.9) for VWFpp/VWF:Ag ratio (Figure 3). The median VWFpp/VWF:Ag ratio was 2.45 (range, 0.79-3.3) for type 2M and 2 for 2A (range, 0.78-3.5).

Protein modeling and structural analysis

Owing to the lack of information about the mutual spatial arrangement of A1 and A2 and the overall system dynamics, we applied Langevin molecular dynamics (LMD) to simulate the overall mutual diffusional properties of the single A1 and A2 domains and thus to simulate the formation of their encounter complex (hereinafter referred as A1-A2). A 200 ns LMD simulation converged from an extended starting structure (supplemental Figure 1A) to a stable complex that was extracted as an average structure from its geometric or energetic plateau (supplemental Figure 1B). It displays

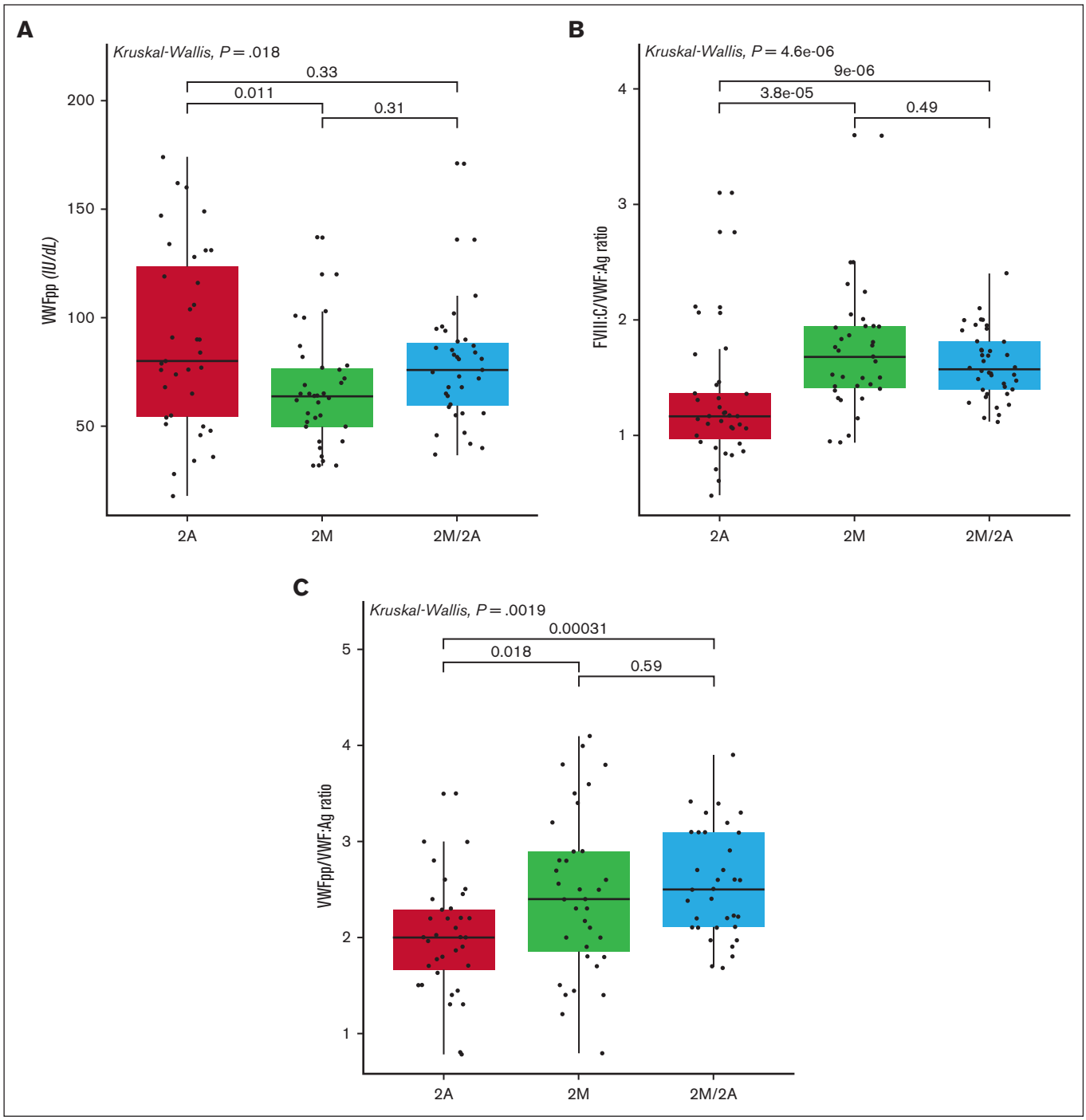

Figure 3. Underlying mechanism in patients with VWD type 2A, 2M, and 2M/2A. (A-B) VWF synthesis and secretion were evaluated with FVIII:C/VWF:Ag ratio and VWFpp antigen. (C) VWF-enhanced clearance was assessed by VWFpp/VWF:Ag ratio. Red indicates type 2A VWD; green indicates type 2M VWD; and blue indicates cases with p.R1315L, p.R1374H, and p.R1374C.

(Figure 4A) a compact arrangement of A1 and A2 domains with residues R1315 and R1374 located at the interface between them. We found that these variants were the only ones that fall at the interface between the A1 and A2 domains.

The wt A1-A2 dynamics display an almost gaussian distribution of the radius of gyration (ROG) and of the backbone atoms RMSD, that is, the major mode ROG equals 2.54 nm and the major mode of RMSD equals 0.38 nm (Figure 4B and C). A minor second mode of both the distributions can be referred to the original configuration because it stems from the final LMD configuration. Upon introducing *VWF* variants in the wt system, the A1-A2 global dynamics follows a different fate for the 2 residues: p.R1315L/C induce more compactness, whereas p.R1374H/C display a more

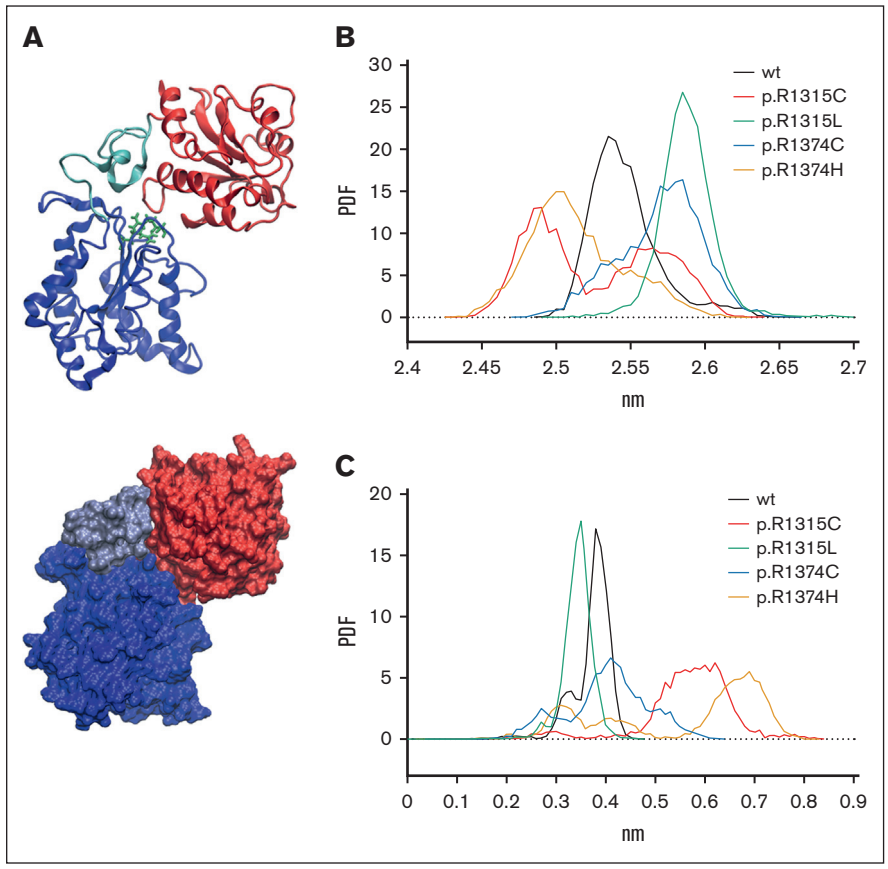

Figure 4. Structure of wt A1-A2 domains and radius of gyration (ROG) and root mean square deviation (RMSD) analysis. (A) Final structure of wt A1-A2 after the Langevin dynamics simulation in cartoon (above) and in molecular surface (below) representation. Domains A1 and A2 are respectively reported in blue and in red, the 1465 to 1494 linker is reported in gray. The residues 1315 and 1374 are reported as green sticks. Analysis shows (B) ROG and (C) RMSD distributions of wt A1-A2 (black) and its mutants (p.R1315C, red; p.R1315L, green; p.R1374C, blue; and p.R1374H, yellow): the single aminoacid comparisons are reported in the small images flanking the global overlap.

extended overall geometry (Figure 4B). The RMSD distributions (Figure 4C) reveal that once residue 1374 is mutated the system's inner dynamics remain on average unaltered. However, residue 1315 highly affects the inner system dynamics with respect to the starting conditions. These 2 general properties allow us to classify the variants according to their macromolecular behaviors, that is, p.R1315L/C are disorder-inducing and compaction-inducing, whereas p.R1374C/H are order-maintaining and extension-inducing. This is also reflected by the intradomain contacts for p.R1374C/H and their increase for p.R1315L/C (supplemental Figure 4). The highest variability of the ROG and of the RMSD (supplemental Figure 5A,C) is observed for the domain containing *VWF* variants (supplemental Figure 5B,D).

The local flexibility of residues was monitored by their Cα root mean square fluctuations (RMSF), that is, the local RMSD expressed using Cα motions as representative of those of the entire residue. As already suggested by the RMSD, the local dynamics ($\Delta RMSF = RMSF_{mutant} - RMSF_{wt}$; Figure 5A; supplemental Figure 5) appears to be broadly influenced through all the A1-A2 sequence, and respectful to RMSDs (Figure 4), p.R1315C/L variants have more perturbing effects than p.R1374C/H. A closer inspection of ΔRMSF reveals that in p.R1315C/L, a long-range effect is displayed by the 1478 to 1488 and the 1345 to 1355 regions. Notably, this effect is not strongly present in p.R1374C/H. However, regardless of the negligible effect of the p.R1374H on the overall system mobility, it induces more rigidity in the 1345 to 1355 region, whereas such effect is not present in pR1374C. This 10-residue stretch corresponds to the contact region of the VWF A1 domain with the D3, as recently highlighted by the cryogenic electron microscopy structure of the D1D2D'D3A1 complex in the context of a reconstituted VWF tubule.[31] As shown in Figure 5, residues 1345 to 1355 (in blue) are in close contact (ie, within 0.75 nm) with residues 895 to 1100 of the D3 domain and with residues 360 to 380 of a close unstructured region.

Principal component analysis (PCA) reduces data noise related to atomic displacements by comparing the conformational space of A1-A2 using their first 2 principal components (PC1 and PC2) (Figure 6A). The populations of structures identified by PCA projections can be assumed as a proxy of the potential energy of a molecular system, hence it is evident that wt A1-A2 and p.R1374H share a common conformational space characterized by a deep stable minimum. Conversely, R1315L, p.R1315C, and R1374C instability is reflected by a pronounced roughness of their PCA projections. The PCA–based representative states (centroids) of the system were compared according to their backbone RMSDs (Figure 6B), that is, the degree of overlap between centroids structures. The most populated centroid of every mutant displays a relatively high RMSD compared with wt A1-A2 (ie, approximately or higher than 5 Å), with the exception of p.R1374H (3.8 Å). This finding is in accordance with the overall time–averaged RMSD. The most striking result from PCA is finding that mutations result in a variety of largely different states. If grouped by mutated residues, the most populated centroids of p.R1315C/L are very structurally similar (3.7 Å) to those of p.R1374C/H (4.7 Å). However, the other

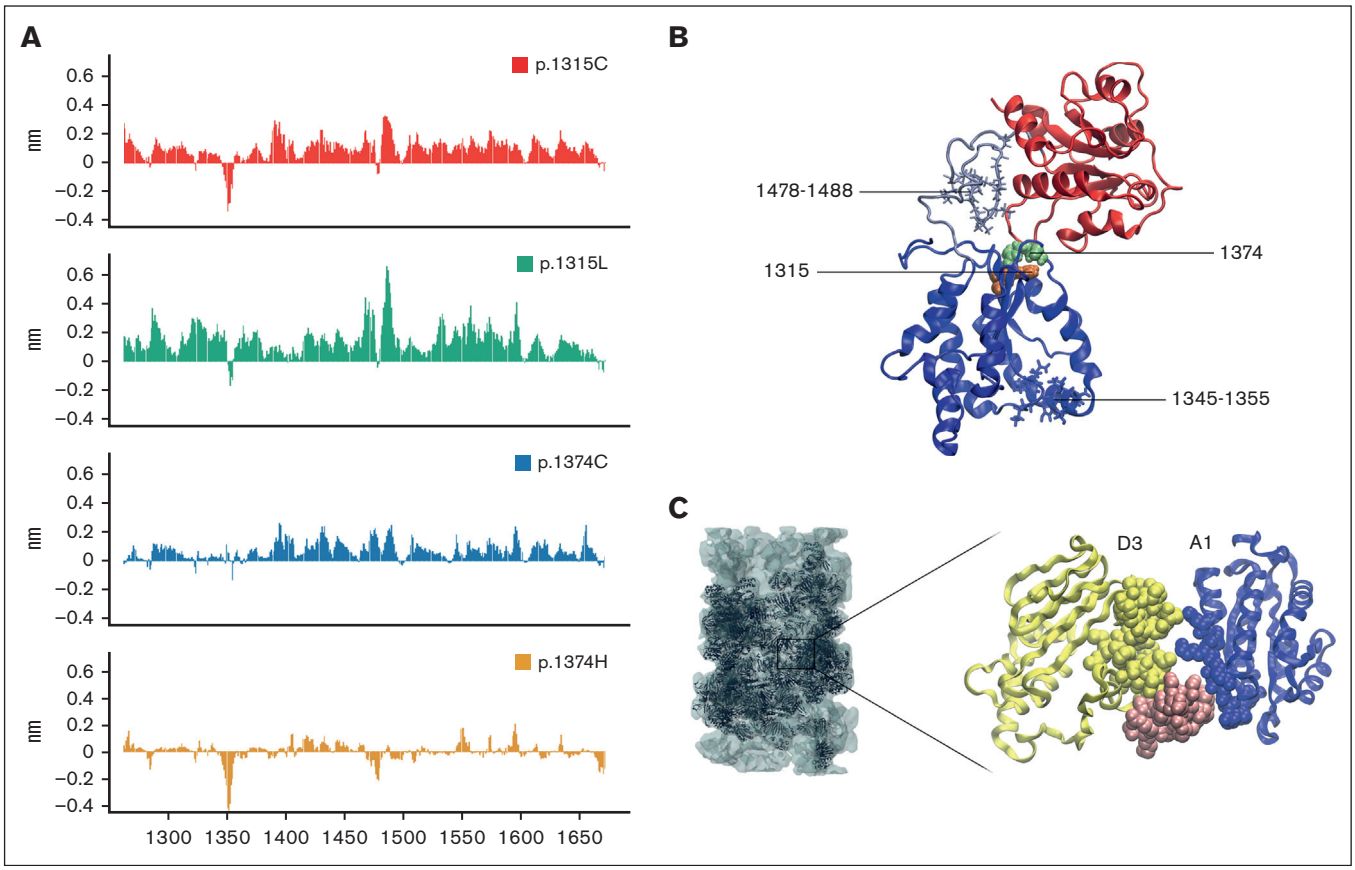

Figure 5. Alpha carbon (Ca) root mean square fluctuations (RMSF) in wt A1-A2 and A1-A2 mutants. (A) Alpha carbon (Ca) RMSF differences between the ones of A1-A2 mutants (p.R1315C, red; p.R1315L, green; p.R1374C, blue; and p.R1374H, yellow) and the ones of wt A1-A2. (B) The largest differences (residues 1345-1355 and residues 1478-1488) are reported on the reference structure of wt A1-A2 alongside the position of mutated residues (lime/orange sticks). The original RMSF values are reported in the supplemental Figure 6. (C) Contacts between A1 and D3 domains of VWF in the context of tubule structure (reference structure: PDB ID 8D3D; the experimental cryogenic electron microscopy data are reported from the RCSB-PDB on the left together with domains). The A1 domain and its residues 1345-1355 are reported in blue, D3 domain and its residues 895-902, 988-999 and 1007-1013 are evidenced in yellow. Residues 344-371 belonging to the VWF (ie, within 0.75 nm of the surfaces of the A1 and D3 domains) without domain assignment are highlighted in brown. Van der Waals surfaces have been used for representing single residues.

minor states of mutants are representatively populated (Figure 6B), and their centroids have a very high RMSD compared with all the most representative centroids of each mutant, with an RMSD always higher than 5.5 Å (Figure 6B).

Discussion

Type 2 VWD is known for its genotype-phenotype correlations in which most of the variants are fully penetrant with a clear phenotypic presentation. Despite this, some variants in several VWD cohorts are associated with different VWD types, and their classification is a matter of debate. We and others so far characterized >300 *VWF* variants and their phenotypic characteristics in patients with type 2 VWD.[8,32-38] Among them, 4 variants (p.R1315L, p.R1315C, p.R1374H, and p.R1374C) often received different VWD classification, such as 2A, 2M, 1C, unclassified, 2A/2M, or 2M/2A. These inconsistencies are partially because of the unavailability of all VWF assays,[39] but also the fact that VWF:CB assay is not standardized and various collagen types are used in different centers. The possibility of performing a densitometric multimer analysis that evaluates high, intermediate, and low MWM proportions appears to be important as well. Genetic testing can also assist in establishing the correct diagnosis for patients suspected of having type 2 VWD.

We conducted this extensive study on a large cohort of patients with these variants to understand their molecular and laboratory phenotype, underlying mechanisms, and their effects on the VWF structure. From a laboratory phenotypic standpoint, we found that patients with p.R1315L, p.R1374H, and p.R1374C variants share some characteristics of both type 2A and 2M. In patients with 2A, VWF:GPIbR/VWF:Ag and VWF:CB/VWF:Ag ratios are dramatically reduced as a result of high and intermediate MWM loss, with an increase in VWF cleavage products (ie, low MWM). However, patients with classical type 2M have only a reduced VWF:GPIbR/VWF:Ag with a full VWF multimeric profile and hence a normal VWF:CB/VWF:Ag ratio. Our cohort with p.R1315L, p.R1374H, and p.R1374C had severely reduced VWF:GPIbR/VWF:Ag and a modest decrease in VWF:CB/VWF:Ag ratios. This can be explained by 2 defects, (1) a reduced VWF A1 domain binding to GPIb and (2) an altered VWF multimeric pattern in which patients showed a slightly

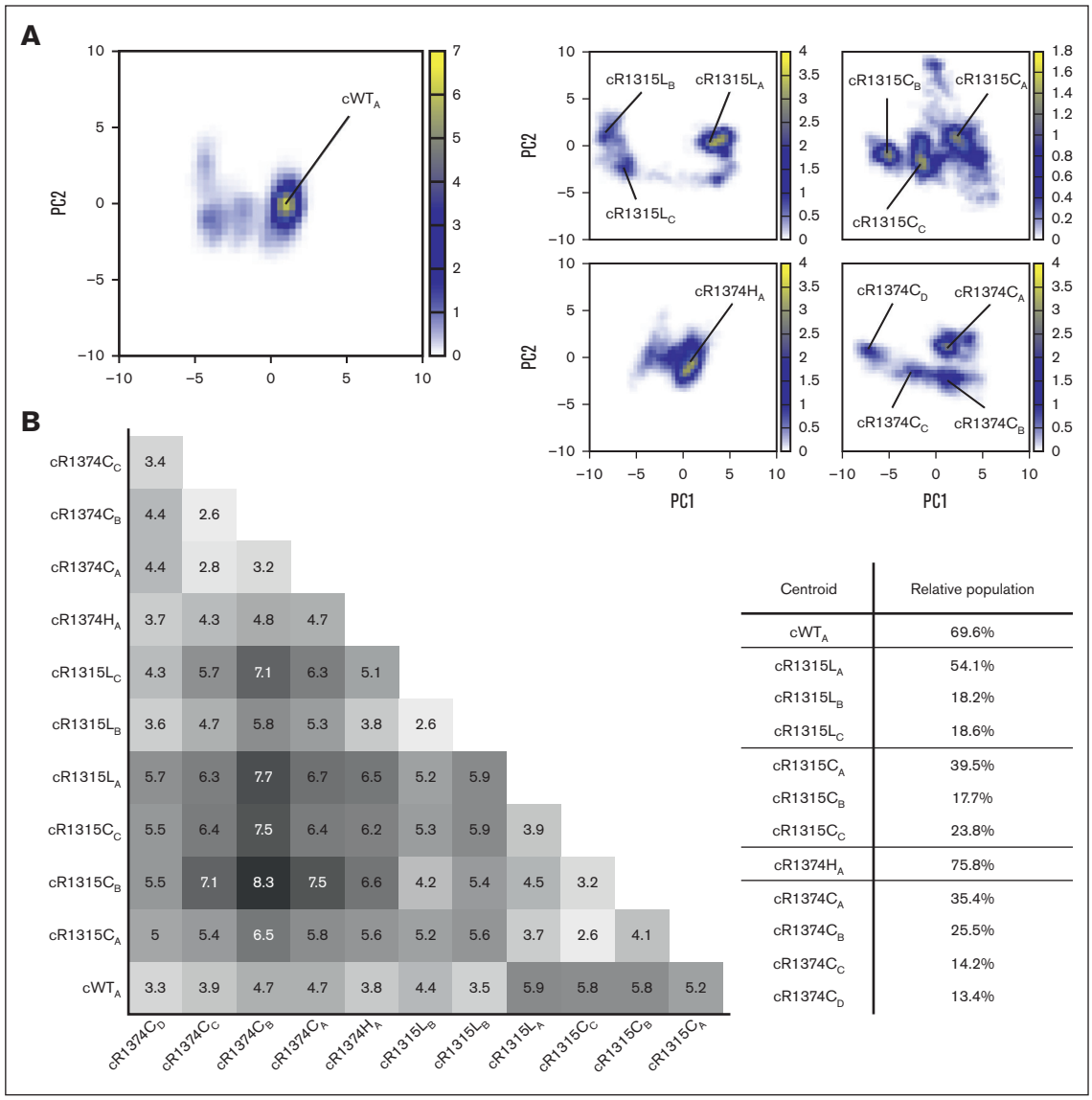

Figure 6. Principal component analysis (PCA) of the molecular dynamics (MD) trajectory of the wt A1-A2 and its mutants. (A) PCA of the MD trajectory of the wt A1-A2 and its 4 mutants (p.R1315C, p.R1315L, p.R1374C, p.R1374H). The principal components 1 and 2 have been used and the density of points has been reported as heat maps (see "Materials and methods" for further details). The most populated centroids have been explicitly indicated. (B) RMSDs between the backbone atoms of PCA-derived centroids. The darkest colors correspond to the highest RMSD values, lightest colors to the lowest RMSD values. The numbers in the box correspond to the values of RMSDs expressed in Å.

diminished proportion of HMWM and little increase of low and intermediate multimers. We believe that the slight reduction of HMWM (characteristic of type 2A) is primarily responsible for marginally reduced VWF:CB/VWF:Ag ratio, whereas the markedly reduced VWF:GPIbR/VWF:Ag ratio is mainly because of a type 2M defect (diminished binding of A1-GPIb). Indeed, Tischer et al previously investigated p.R1374H using several laboratory and rheological tools and their results clearly showed that the recombinant A1 carrying this variant did not bind to GPIba at any shear rate and they classified it as type 2M.[40] The PCM-EVW-ES of Spain classified p.R1374H as type 2A because of the observed abnormal multimers and p.R1374C as 2A/2M.[32] On closer examination, their data showed that most patients had a slight HMWM loss, very low VWF:GPIbR/VWF:Ag ratios, and a mild reduction in VWF:CB/VWF:Ag ratio, consistently with our results. However, because the defect of these patients is mainly due to the decreased A1 binding to GPIb (2M) and only partially to the HMWM loss (2A), we suggest calling them type 2M/2A, rather than 2A/2M. In a recent study from the Zimmerman cohort, p.R1374H and p.R1374C were diagnosed as type 2A or type 1C.[36] In addition to reduced VWF:GPIbR/VWF:Ag ratio, our densitometry analysis of VWF multimers confirmed the slight reduction of HMWM, thus excluding a type 1 phenotype. p.R1374C is another variant with inconsistent VWD classification. Two cohorts from France classified p.R1374C and p.R1374H as 2A/2M[41] and type 2M.[33] In vitro homozygous

expression study of p.R1374C showed a type 2A phenotype, although with a normal expression as heterozygous recombinant VWF, suggesting shared features of this variant with both type 2A and 2M.[42] Among our 7 cases with p.R1374C, again, a mild reduction of VWF:CB/VWF:Ag ratio (median, 0.52), greatly reduced VWF:GPIbR/VWF:Ag ratio (median, 0.37) and slight reduction of HMWM was observed. This variant reported to be a frequent VWD variant in Northwest of Spain,[43] with a quantitative distribution of multimers in between the normal and the 2A VWF. Variant p.R1315L has been reported as type 1,[44] 2A,[32,44] 2M,[45] and 2A (IIE).[46] The single case of Spain VWD cohort carrying p.R1315L had a very low VWF:GPIbR/VWF:Ag ratio (0.24) and a mild reduction of VWF:CB/VWF:Ag ratio (0.66) along with diminished HMWM.[32] These results were comparable with our 7 cases (median ratios of 0.45 and 0.57 with slight loss of HMWM), indicating a phenotype between type 2M and 2A. We had 3 cases with p.R1315C and all showed type 2M characteristics, that is, low VWF:GPIbR/VWF:Ag ratio (0.3, 0.41, and 0.5), normal VWF:CB/VWF:Ag ratio (0.93, 0.8, and 0.71), and normal multimeric pattern.

We found a reduced VWF synthesis or secretion in type 2M and the cohort with p.R1315L, p.R1374H, and p.R1374C, but with no apparent synthesis or secretion defect for most type 2A cases. All the 40 cases with p.R1315L, p.R1374H, and p.R1374C had an elevated VWFpp/VWF:Ag ratio, suggesting that enhanced VWF clearance is a common etiology in these variants. Owing to the markedly enhanced clearance, these variants have also been reported as type 1C.[36]

Although p.R1315C had type 2M characteristics, we chose to report this variant effect along with the 3 other variants (p.R1315L, p.R1374H, and p.R1374C) on the VWF structure. What clearly characterizes these 4 variants, among the other type 2 variants, is their structural uniqueness. Indeed, they are the only variants that fall at the interface between the A1 and A2 domains. We can assume that all the mutants that exhibit a distinct classification of VWD fall everywhere along the sequence but not in the A1-A2 contact region, so that they can be considered independent of each other in regulating the VWF interactions. In contrast, the position of residues R1315 and R1374 at the A1-A2 interface ensures a mutual alteration in motion and in the binding abilities of the 2 domains: the intermediate phenotype 2M/2A can be supported at the molecular level owing to a geometry that makes A1 and A2 dependent on each other.

We were able to detect a subclassification among the 4 variants studied in the present work. p.R1315C/L induces more compactness and increased internal mobility, but p.R1347H/C looks more extended with an overall mobility comparable with that of the wt A1-A2. A closer assessment of local features of internal motion confirms the impact of these variants on the overall A1-A2 dynamics with long-range effects: p.R1315C, p.R1315L, and p.R1347H show a reduced mobility of the regions 1345 to 1355 (almost unchanged in p.R1374C). This was recently demonstrated to modulate the newly discovered interaction with the VWF D3 domain in the context of the tubular Weibel–Palade bodies. Such a mobility reduction can partially explain the alteration of VWF multimerization and release from tubules and the consequent variation of plasma VWF multimers and levels. These findings can be supported by our phenotypic results, showing an overall reduction in VWF synthesis and mild multimer defects. However, the region involved in the complex formation with GPIb (residues, 1325-1328)[47] does not seem to be heavily altered by these 4 variants.

Mutations produce a wide variety of accessible states, which are evident in the mobility analysis using PCA. These data revealed that the common pathological trait from a structural point of view can be related to the accessibility of sensibly populated states, the exploration of which is induced by mutations. p.R1374H constitutes an exception, although an Arginine/Histidine substitution does not alter the chemical profile of the amino acid environment, but the pathological profile is provided by the long-range effect on the region involved in the tubule formation or stability.

In conclusion, we propose a new classification for p.R1315L, p.R1374H, and p.R1374C as type 2M/2A VWD, because they present a shared phenotype between types 2M and 2A, but their pathophysiology seems to be influenced most by type 2M (hence, 2M/2A). Variant p.R1315C clearly showed a type 2M phenotype but with a similar structural effect on VWF as p.R1315L, p.R1374H, and p.R1374C. Our deep structural analysis indicates the unique location of these 4 variants on the A1-A2 domains and their distinctive effect on VWF structure.

Acknowledgments

The authors acknowledge P.M. Mannucci for his critical advice in the preparation of this manuscript and L.F. Ghilardini for the illustration work. The Fondazione IRCCS Ca' Granda Ospedale Maggiore Policlinico is a member of the European Reference Network EuroBloodNet.

This work was partially supported by the Italian Ministry of Health (Bando Ricerca Corrente 2022).

Authorship

Contribution: O.S. designed the study, collected and analyzed data, and wrote the manuscript; L.M. and S.Z. performed protein modeling predictions and structural biology and wrote the manuscript; A.C., M.T.P., P.C., and G.C. performed the laboratory tests; S.M.S. and A.C. were involved in the patient's evaluation; L.B. and F.P. critically revised the manuscript; and all authors have approved the final manuscript.

Conflict-of-interest disclosure: F.P. serves on the advisory committees of CSL Behring, Biomarin, Roche, Sanofi, and Sobi, and participated in educational meetings/symposia of Takeda/Spark. The remaining authors declare no competing financial interests.

ORCID profiles: O.S., 0000-0002-6630-7879; P.C., 0000-0003-4180-6011; G.C., 0000-0002-0267-3773; M.T.P., 0000-0003-0778-2271; S.M.S., 0000-0002-8456-7519; F.P., 0000-0001-7423-9864.

Correspondence: Flora Peyvandi, Department of Pathophysiology and Transplantation, Fondazione IRCCS Ca'Granda Ospedale Maggiore Policlinico, Angelo Bianchi Bonomi Hemophilia and Thrombosis Center, Università degli Studi di Milano, Via Pace 9, 20122 Milan, Italy; email: flora.peyvandi@unimi.it.

References

1. Rodeghiero F, Castaman G, Dini E. Epidemiological investigation of the prevalence of von Willebrand's disease. *Blood*. 1987;69(2):454-459.
2. Werner EJ, Broxson EH, Tucker EL, Giroux DS, Shults J, Abshire TC. Prevalence of von Willebrand disease in children: a multiethnic study. *J Pediatr*. 1993;123(6):893-898.
3. Bowman M, Hopman W, Rapson D, Lillicrap D, James P. The prevalence of symptomatic von Willebrand disease in primary care practice. *J Thromb Haemostasis*. 2010;8(1):213-216.
4. Bloom AL. *von Willebrand factor: clinical features of inherited and acquired disorders. Mayo Clinic Proceedings; 1991*. Elsevier; 1991:743-751.
5. Seidizadeh O, Cairo A, Baronciani L, Valenti L, Peyvandi F. Population-based prevalence and mutational landscape of von Willebrand disease using large-scale genetic databases. *NPJ Genom Med*. 2023;8(1):31.
6. Sadler J, Budde U, Eikenboom J, et al. Update on the pathophysiology and classification of von Willebrand disease: a report of the Subcommittee on von Willebrand Factor. *J Thromb Haemostasis*. 2006;4(10):2103-2114.
7. James PD, Connell NT, Ameer B, et al. ASH ISTH NHF WFH 2021 guidelines on the diagnosis of von Willebrand disease. *Blood Adv*. 2021;5(1):280-300.
8. Seidizadeh O, Baronciani L, Pagliari MT, et al. Phenotypic and genetic characterizations of the Milan cohort of von Willebrand disease type 2. *Blood Adv*. 2022;6(13):4031-4040.
9. Seidizadeh O, Peyvandi F, Mannucci PM. Von Willebrand disease type 2N: an update. *J Thromb Haemostasis*. 2021;19(4):909-916.
10. Mannucci P, Lombardi R, Bader R, et al. Heterogeneity of type I von Willebrand disease: evidence for a subgroup with an abnormal von Willebrand factor. *Blood*. 1985;66(4):796-802.
11. Flood VH, Christopherson PA, Gill JC, et al. Clinical and laboratory variability in a cohort of patients diagnosed with type 1 VWD in the United States. Blood. *Blood*. 2016;127(20):2481-2488.
12. Federici AB, Canciani MT, Forza I, et al. A sensitive ristocetin co-factor activity assay with recombinant glycoprotein Ibalpha for the diagnosis of patients with low von Willebrand factor levels. *Haematologica*. 2004;89(1):77-85.
13. Bowyer AE, Goodfellow KJ, Seidel H, et al. Evaluation of a semi-automated von Willebrand factor multimer assay, the Hydragel 5 von Willebrand multimer, by two European Centers. *Res Pract Thromb Haemost*. 2018;2(4):790-799.
14. Seidizadeh O, Ciavarella A, Baronciani L, et al. Clinical and laboratory presentation and underlying mechanism in patients with low VWF. *Thromb Haemostasis*. Published online 2 November 2023. https://doi.org/10.1055/a-2186-6362
15. Seidizadeh O, Baronciani L, Pagliari MT, et al. Genetic determinants of enhanced von Willebrand factor clearance from plasma. *J Thromb Haemostasis*. 2023;21(5):1112-1122.
16. Baronciani L, Cozzi G, Canciani MT, et al. Molecular characterization of a multiethnic group of 21 patients with type 3 von Willebrand disease. *Thromb Haemostasis*. 2000;84(4):536-540.
17. Baronciani L, Cozzi G, Canciani MT, et al. Molecular defects in type 3 von Willebrand disease: updated results from 40 multiethnic patients. *Blood Cells Mol Dis*. 2003;30(3):264-270.
18. Baronciani L, Peake I, Schneppenheim R, et al. Genotypes of European and Iranian patients with type 3 von Willebrand disease enrolled in 3WINTERS-IPS. *Blood Adv*. 2021;5(15):2987-3001.
19. Lee HT, Park UB, Jeong TJ, et al. High-resolution structure of the vWF A1 domain in complex with caplacizumab, the first nanobody-based medicine for treating acquired TTP. *Biochem Biophys Res Commun*. 2021;567:49-55.
20. Zhang Q, Zhou Y-F, Zhang C-Z, Zhang X, Lu C, Springer TA. Structural specializations of A2, a force-sensing domain in the ultralarge vascular protein von Willebrand factor. *Proc Natl Acad Sci U S A*. 2009;106(23):9226-9231.
21. Jumper J, Evans R, Pritzel A, et al. Highly accurate protein structure prediction with AlphaFold. *Nature*. 2021;596(7873):583-589.
22. Tanner DE, Chan K-Y, Phillips JC, Schulten K. Parallel generalized Born implicit solvent calculations with NAMD. *J Chem Theor Comput*. 2011;7(11):3635-3642.
23. Phillips JC, Hardy DJ, Maia JD, et al. Scalable molecular dynamics on CPU and GPU architectures with NAMD. *J Chem Phys*. 2020;153(4):044130.
24. Brooks BR, Bruccoleri RE, Olafson BD, States DJ, Swaminathan Sa, Karplus M. CHARMM: a program for macromolecular energy, minimization, and dynamics calculations. *J Comput Chem*. 1983;4(2):187-217.
25. Abraham MJ, Murtola T, Schulz R, et al. GROMACS: High performance molecular simulations through multi-level parallelism from laptops to supercomputers. *SoftwareX*. 2015;1-2:19-25.
26. Lindorff-Larsen K, Piana S, Palmo K, et al. Improved side-chain torsion potentials for the Amber ff99SB protein force field. *Proteins*. 2010;78(8):1950-1958.
27. Jorgensen WL, Chandrasekhar J, Madura JD, Impey RW, Klein ML. Comparison of simple potential functions for simulating liquid water. *J Chem Phys*. 1983;79(2):926-935.
28. Jaidhan B, Rao PS, Apparao A. Energy minimization and conformation analysis of molecules using steepest descent method. *Int J Comput Sci Inf Technol*. 2014;5(3):3525-3528.

29. Hess B, Bekker H, Berendsen HJ, Fraaije JG. LINCS: a linear constraint solver for molecular simulations. *J Comput Chem*. 1997;18(12):1463-1472.

30. Humphrey W, Dalke A, Schulten K. VMD: visual molecular dynamics. *J Mol Graph*. 1996;14(1):33-28.

31. Javitt G, Fass D. Helical self-assembly of a mucin segment suggests an evolutionary origin for von Willebrand factor tubules. *Proc Natl Acad Sci U S A*. 2022;119(15):e2116790119.

32. Borràs N, Batlle J, Pérez-Rodríguez A, et al. Molecular and clinical profile of von Willebrand disease in Spain (PCM-EVW-ES): comprehensive genetic analysis by next-generation sequencing of 480 patients. *Haematologica*. 2017;102(12):2005-2014.

33. Veyradier A, Boisseau P, Fressinaud E, et al. A laboratory phenotype/genotype correlation of 1167 French patients from 670 families with von Willebrand disease: a new epidemiologic picture. *Medicine*. 2016;95(11):e3038.

34. Yadegari H, Driesen J, Pavlova A, Biswas A, Hertfelder H-J, Oldenburg J. Mutation distribution in the von Willebrand factor gene related to the different von Willebrand disease (VWD) types in a cohort of VWD patients. *Thromb Haemostasis*. 2012;108(4):662-671.

35. Atiq F, Boender J, van Heerde WL, et al. Importance of genotyping in von Willebrand disease to elucidate pathogenic mechanisms and variability in phenotype. *HemaSphere*. 2022;6(6):e718.

36. DiGiandomenico S, Christopherson PA, Haberichter SL, et al. Laboratory variability in the diagnosis of type 2 VWD variants. *J Thromb Haemostasis*. 2021;19(1):131-138.

37. Ahmad F, Jan R, Kannan M, et al. Characterisation of mutations and molecular studies of type 2 von Willebrand disease. *Thromb Haemostasis*. 2013;109(1):39-46.

38. Freitas SdS, Rezende SM, de Oliveira LC, et al. Genetic variants of VWF gene in type 2 von Willebrand disease. *Haemophilia*. 2019;25(2):e78-e85.

39. Favaloro EJ, Pasalic L, Curnow J. *Type 2M and Type 2A von Willebrand disease: similar but different. Seminars in Thrombosis and Hemostasis; 2016*. Thieme Medical Publishers; 2016:483-497.

40. Tischer A, Madde P, Moon-Tasson L, Auton M. Misfolding of vWF to pathologically disordered conformations impacts the severity of von Willebrand disease. *Biophys J*. 2014;107(5):1185-1195.

41. Fressinaud E, Mazurier C, Meyer D. Molecular genetics of type 2 von Willebrand disease. *Int J Hematol*. 2002;75(1):9-18.

42. Doruelo AL, Haberichter SL, Christopherson PA, et al. Clinical and laboratory phenotype variability in type 2M von Willebrand disease. *J Thromb Haemostasis*. 2017;15(8):1559-1566.

43. Penas N, Pérez-Rodríguez A, Torea JH, et al. von Willebrand disease R1374C: type 2A or 2M? A challenge to the revised classification. High frequency in the northwest of Spain (Galicia). *Am J Hematol*. 2005;80(3):188-196.

44. Favaloro E. Genetic testing for von Willebrand disease: the case against. *J Thromb Haemostasis*. 2010;8(1):6-12.

45. Gadisseur A, Berneman Z, Schroyens W, Michiels JJ. Laboratory diagnosis of von Willebrand disease type 1/2E (2A subtype IIE), type 1 Vicenza and mild type 1 caused by mutations in the D3, D4, B1–B3 and C1–C2 domains of the von Willebrand factor gene: role of von Willebrand factor multimers and the von Willebrand factor propeptide/antigen ratio. *Acta Haematol*. 2009;121(2-3):128-138.

46. Michiels J, Smejkal P, Zapletal O, Penka M, Blatny J. Determination of two rapid von Willebrand factor (VWF) activity assays VWF: Gpibm and VWF: Gpibr in well defined von Willebrand disease patients using a complete set of classical and sensitive VWF assays. *J Hematol Thrombo Dis*. 2019;6(299):2-15.

47. Blenner MA, Dong X, Springer TA. Structural basis of regulation of von Willebrand factor binding to glycoprotein Ib. *J Biol Chem*. 2014;289(9):5565-5579.